SUPPORTING INFORMATION

Defect-Engineered Surfaces to Investigate the Formation of Self-Assembled Molecular Networks

Li-Hua Yu [a], Zhen-Feng Cai [d], Lander Verstraete [a, e], Yuanzhi Xia [a], Yuan Fang [c,f], Louis Cuccia [g], Oleksandr Ivasenko [a,b,c] *, Steven De Feyter [a]*

[a.] *Department of Chemistry, Division of Molecular Imaging and Photonics, KU Leuven, Celestijnenlaan 200F, B-3001 Leuven, Belgium. E-mail: steven.defeyter@kuleuven.be*

[b.] *Institute of Functional Nano & Soft Materials (FUNSOM), Joint International Research Laboratory of Carbon-Based Functional Materials and Devices, Soochow University, Suzhou, 215123, Jiangsu, PR China. E-mail: ivasenko@suda.edu.cn*

[c.] *Jiangsu Key Laboratory for Carbon-Based Functional Materials & Devices, Institute of Functional Nano & Soft Materials (FUNSOM), Soochow University, Suzhou 215123, P. R. China.*

[d.] *Department of Chemistry and Applied Biosciences, ETH Zurich, Zurich CH-8093, Switzerland.*

[e.] *imec, Kapeldreef 75, 3001 Leuven, Belgium.*

[f.] *Jiangsu Key Laboratory of Advanced Negative Carbon Technologies, Soochow University, Suzhou, 215123, Jiangsu, PR China.*

[g.] *Department of Chemistry and Biochemistry, Concordia University, 7141 Sherbrooke St. W., Montreal, Québec, Canada.*

Corresponding authors:

E-mail: ivasenko@suda.edu.cn, steven.defeyter@kuleuven.be

S1. Self-assembly of QZ-C16 on pristine graphite

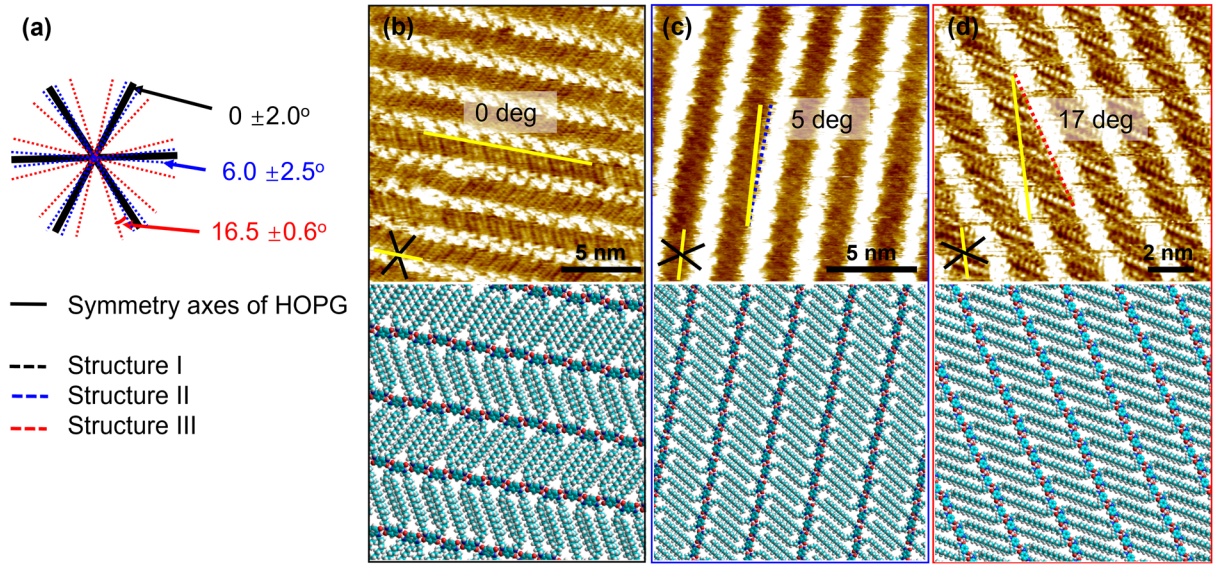

Figure S1. Overview of three structures of QZ-C16 SAMNs at the 1-phenyloctane/HOPG interface. (a) Black lines show the three main symmetry axes of HOPG. Black, blue and red dashed lines indicate the orientation of the lamella of structure I, II, III, which are 0 ± 2.0°, 6.0 ± 2.5°, 16.5 ± 0.6°, respectively, with respect to symmetry axes of the graphite lattice (1 0 0) (yellow line). (b-d) The high-resolution STM images show three structures. The orientations of the lamellae are indicated inside images, the proposed molecular models show three packing structures, specifically the angle between the alkyl chain and the head group is different for the three structures.

Table S1. Unit cell dimensions for three structures of QZ-C16 SAMNs, where '***a***' is the unit cell vector along the head-group row, '***b***' is the unit cell vector connecting adjacent head-group rows, '***γ***' is the unit cell angle, and '***β***' is the alkyl chain to head group row intersecting angle.

Structure	a (nm)	b (nm)	γ (°)	β (°)
I	1.50 ± 0.04	2.59 ± 0.02	79 ± 2	60 ± 2
II	1.48 ± 0.01	2.67 ± 0.03	76 ± 2	67 ± 1
III	1.48 ± 0.01	2.32 ± 0.08	73 ± 2	45 ± 1

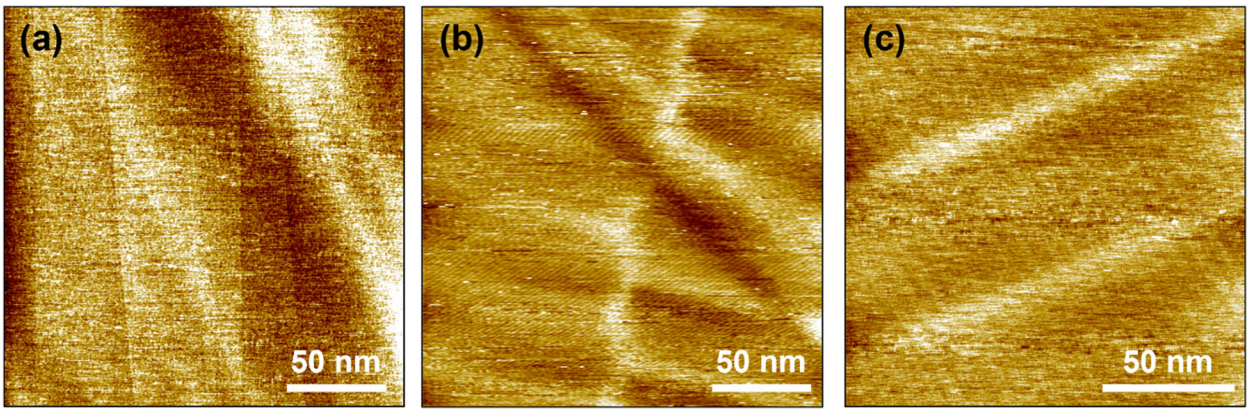

Figure S2. After applying a droplet of QZ-C16 solution (at concentration 10^{-6} M) on the pristine HOPG surface, no QZ-C16 SAMNs could be detected (representative images of empty graphite are shown in a). Occasionally observed highly periodic linear patterns (50-600Hz) that uniformly span the full image width were attributed to electromagnetic and audio noise from nearby circuits (shown as b, c). Imaging conditions: $V_s = -0.8$ V, $I_t = 0.08$ nA.

S2. Self-assembly of QZ-C16 on the CM-HOPG surface.

Estimate the grafting density of the surface by SPIP software.

SPIP software is commercially available, all the grafting densities were estimated following the same procedures. First, open an STM image file, and perform "Plane Correction''; after that, "Particle & Pore Analysis'' will be conducted, the grafted molecules could be identified easily due to the different contrast with the substrate background; at last, the parameters of the grafted pins, in terms of the number, area, diameter, ~~mean high~~ and so on, are recorded automatically.

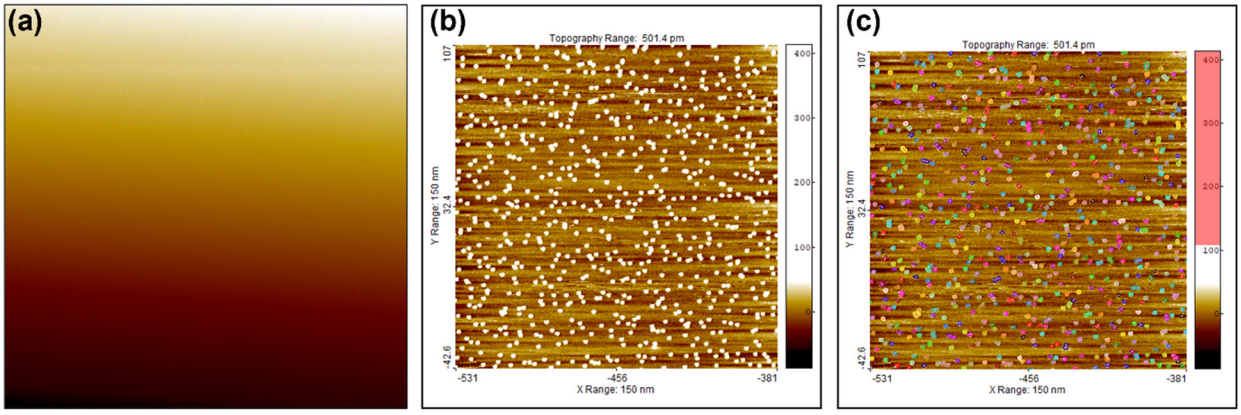

Figure S3. (a) The initial STM image. (b) STM image after performing global correction and line-wise correction. The contrast of the image could be adjusted by the color scale (on the right). (c) STM image where the grafted pins were highlighted.

Determination of the surface coverage and Langmuir adsorption isotherm.

The surface coverage ($\boldsymbol{\theta}$) of QZ-C16 defined in individual STM images on bare HOPG can be directly measured as the area occupied by its self-assembly ($\boldsymbol{A}_{\text{assemblies}}$) divided by the total available area for size of the image ($\boldsymbol{A}_{\text{image}}$), $\boldsymbol{\theta} = \boldsymbol{A}_{\text{assemblies}}/\boldsymbol{A}_{\text{image}}$. However on CM-HOPG samples, we have to take into account that the grafted molecules ($\boldsymbol{A}_{\text{total grafs}}$) reduces the available area for molecular assembly, so $\boldsymbol{\theta} = \boldsymbol{A}_{\text{assemblies}}/(\boldsymbol{A}_{\text{image}} - \boldsymbol{A}_{\text{total graft}})$, where $\boldsymbol{A}_{\text{total grafs}} = \boldsymbol{N}_{\text{grafts}} * \boldsymbol{A}_{\text{single graft}}$, $\boldsymbol{N}_{\text{grafts}}$ is the measured number of grafts in each image. Furthermore, $\boldsymbol{A}_{\text{single graft}} = 1.34 \pm 0.66$ nm^2 is a measured area blocked by individual graft at low grafting density (~45000 grafts/μm^2), but when pits aggregate or get close to each other, their actual occupied area is much larger than the sum of the size of each single pin. As an approximation we used $\boldsymbol{A}_{\text{single graft}} = 2.9$ nm^2, since at this value $\boldsymbol{\theta}$ gave the smallest standard deviation throughout the whole data set (all concentrations and all recorded images).

In condensed phases (solutions), adsorption to a solid surface is a competitive process between the solvent and the solute to occupy binding sites. The relationship between the amount of adsorption and the concentration of solute (adsorbate) in solution at equilibrium is often described by the Langmuir adsorption isotherm:

$$\boldsymbol{\theta}=\frac{\boldsymbol{K}*\boldsymbol{c}}{\boldsymbol{1}+\boldsymbol{K}*\boldsymbol{c}} \qquad (1)$$

In this equation, $\boldsymbol{c_{eq}}$ is the solution concentration of QZ-C16 after the adsorption-desorption equilibrium is reached. For our typical measuring conditions, the equilibrium concentration as a function of surface coverage: $\boldsymbol{c_{eq}=c_0-\theta * A_{empty}/(N_A*V*A}$ $_{\text{single molecule}}$), where $\boldsymbol{c_0}$ is the initial concentration of QZ-C16 stock solutions, $\boldsymbol{\theta}$ is the surface coverage of adsorbed QZ-C16 molecules, $\boldsymbol{A_{empty}}$ is the empty area that is accessible for molecules to assemble on the substrate; $\boldsymbol{N_A}$ is Avogadro's number, and $\boldsymbol{V}$ is the volume of QZ-C16 solution in contact with the graphite (~5-18 μL, the maximum value was used here to estimate the equilibrium concentration); $\boldsymbol{A}_{\text{single molecule}}$ is the size of the single molecule, which is estimated by the unit cell parameter. $\boldsymbol{A_{empty}}$ was estimated by: $\boldsymbol{A_{empty}=A_{sample}-N_{grafts}*A_{single\ graft}*A_{grafting\ area}/A_{image}}$, where $\boldsymbol{A_{sample}}$ =1.44×10^{-4} m^2 which is the size of ~ 12 mm × 12 mm HOPG substrate; $\boldsymbol{A_{grafting}}$ is the area that modified by grafts.

Table S2. Surface coverage of QZ-C16 assembly on the CM-HOPG surface at different concentrations.

Initial concentration c_0 (M)	**Equilibrium concentration[1] c_{eq} (M)**	**Surface coverage[2] θ**	**Standard deviation of θ**
5×10^{-7}	3.93×10^{-7}	0.014	0.011
1×10^{-6}	4.08×10^{-7}	0.083	0.095
1×10^{-5}	4.49×10^{-6}	0.72	0.088
1×10^{-4}	9.61×10^{-5}	0.53	0.16
1×10^{-3}	9.93×10^{-4}	0.96	0.11

[1]The equilibrium concentrations were estimated assuming a maximum of 18 μL of corresponding solutions were in full contact with 1.44 cm^2 of the substrate and that the self-assembly surface coverage measured in the central grafted zone of the substrate can be used as an approximation of the surface coverage of QZ-C16 on bare HOPG area that was not grafted.

[2]The surface coverage $\boldsymbol{\theta}$ was estimated in the grafted zone using $\boldsymbol{A}_{\text{single graft}}$ = 2.9 nm^2. In this study, we also assume that $\boldsymbol{\theta}$ is independent on the grafting density and it only changes with the concentration.

Criteria for manually determining the QZ-C16 domains.

Automatic detection of the QZ-C16 domain on CM-HOPG surface was not sufficiently reliable because the presence of grafted species will cause the high contrast variation. Therefore, each domain was manually identified according to one or more criteria described below. Only if assigned to QZ-C16, its parameters were entered for the data analysis:

1) Clear images with a sub-molecular resolution for unambiguous assignment. Such images also serve as references of QZ-C16 appearances in topography and current channels at different imaging conditions.

2) Stripe patterns if they match the alignment and periodicity of QZ-C16 lamellas (2.40 ± 0.2 nm).

3) Sequential imaging of domain growth. It was used to corroborate the QZ-C16 nature of small domains by positively identifying the QZ-C16 stripes in larger domains that were observed in sequential images.

4) Classification of STM contrast features in topography and current channels: in a few cases (e.g. when small domains consisted of a single stripe), tentative sorting was done based on a careful comparison of the observed STM contrast with that of previously confirmed QZ-C16, contaminations or scanning artifacts. Thus, we noticed that QZ-C16 differs from typical contaminations by having brighter rows of quinonimine moieties between darker rows of alkyl chains. From our experience of imaging QZ-C16 and many other assemblies at the HOPG-solution interface, the typical contaminations (presumably originating from residues of scotch tape used for HOPG cleaving and/or grease from the contaminated surface during solution deposition) usually have lower contrast variations (aliphatic nature), different pattern structure and irregular width (probably, due to the polydispersity of polymeric constituents). Since grafts are the tallest and brightest features in such images, the STM feedback optimized for imaging lower contrast QZ-C16 inevitably results in imaging and/or image processing artifacts: e.g., the commonly observed “shadows” next to the grafts. When combined with sporadic current fluctuations along fast scan direction, such artifacts may be confused for “the low-resolution images of single lamellae domains of QZ-C16”. To avoid ambiguity, we assigned all such cases as images of artifacts and exclude them from further analysis.

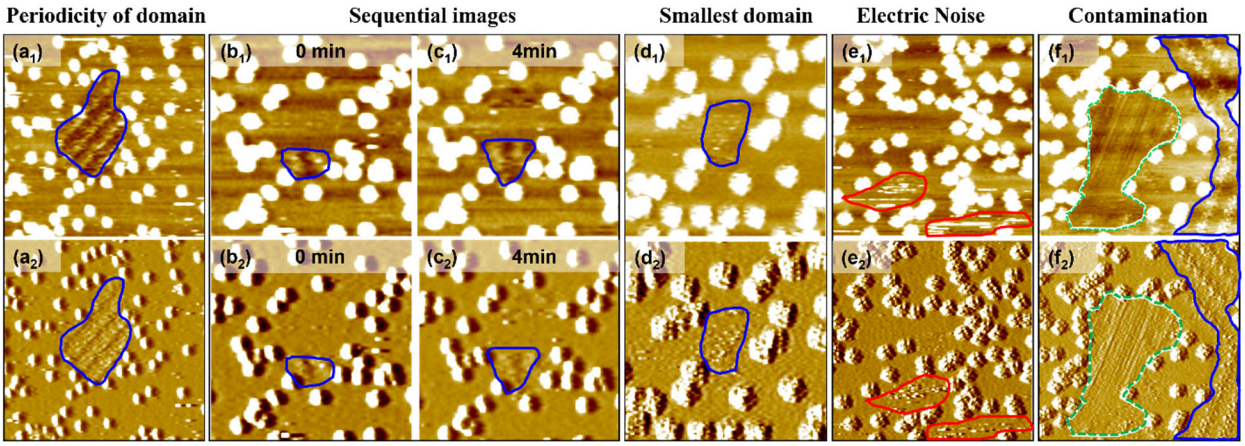

Figure S4. Topography (a_1-f_1) and current (a_2-f_2) STM images show the self-assembly of QZ-C16 (a_1-d_2, f_1, f_2), coloured in blue; the electric noise (e_1, e_2) coloured in red; and the contaminations (f_1, f_2) coloured in green, on CM-HOPG at concentration 10^{-6} M.

Table S3. 8 sets of detailed statistics grouped by the grafting density show the smallest and largest domain size, the domain size with the highest probability, the total number of obtained domains and images of QZ-C16 (10^{-6} M) on the CM-HOPG surface, the average domain size and the surface density of domains.

Grafting density (per 0.01 μm²)	Smallest size of domain (nm²)	Largest size of domain (nm²)	Most probable size of domain (nm²)	Total number of domains	Total number of images	Average size of domain (nm²)	Surface density of domains
250 – 450	93.4	5598	<500	396	181	751.3	1.5
450 – 650	38.5	2877	<300	519	176	331.8	2.2
650 – 850	18.2	825	105 ± 35	543	76	129.2	5.7
850 – 1050	11.6	372	60 ± 20	802	92	77.6	8.0
1050 – 1250	12.7	326	45 ± 15	383	47	60.3	7.6
1250 – 1650	11.0	227	30 ± 10	240	46	48.6	11.5
1650 – 2050	10.4	155	24 ± 8	213	35	33.2	13.3
>2050	11.9	92	25 ± 5	195	35	31.3	12.1

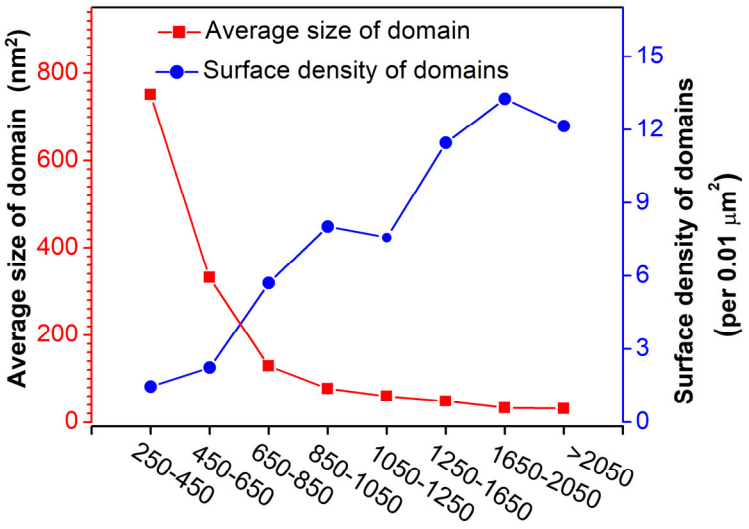

Figure S5. Line plots of the average domain size (red line) and the surface density of obtained domains per 0.01 μm^2 (blue line) for substrates with various grafting densities.

Table S4. 10 sets of detailed statistics containing a similar number of domains show the smallest and largest domain size, the medium size of domain, the average domain size and the total number of obtained domains of QZ-C16 (10^{-6} M) on the CM-HOPG surface.

Grafting density (per 0.01 μm^2)	**Smallest size of domain (nm^2)**	**Largest size of domain (nm^2)**	**Medium size of domain (nm^2)**	**Average size of domain (nm^2)**	**Total number of domains**
<416	93.4	5598	496.0	798.6	330
416-546	38.5	2877	263.0	398.7	331
546-685	40.9	2645	169.0	266.6	354
685-832	18.2	825	104.0	128.1	317
832-876	26.0	372	74.7	89.0	325
876-968	11.6	314	67.9	76.6	325
968-1081	12.9	219	64.6	71.5	333
1081-1307	12.7	326	53.3	58.6	329
1307-1904	10.4	205	34.8	42.5	331
>1904	11.9	95.8	30.0	32.6	319

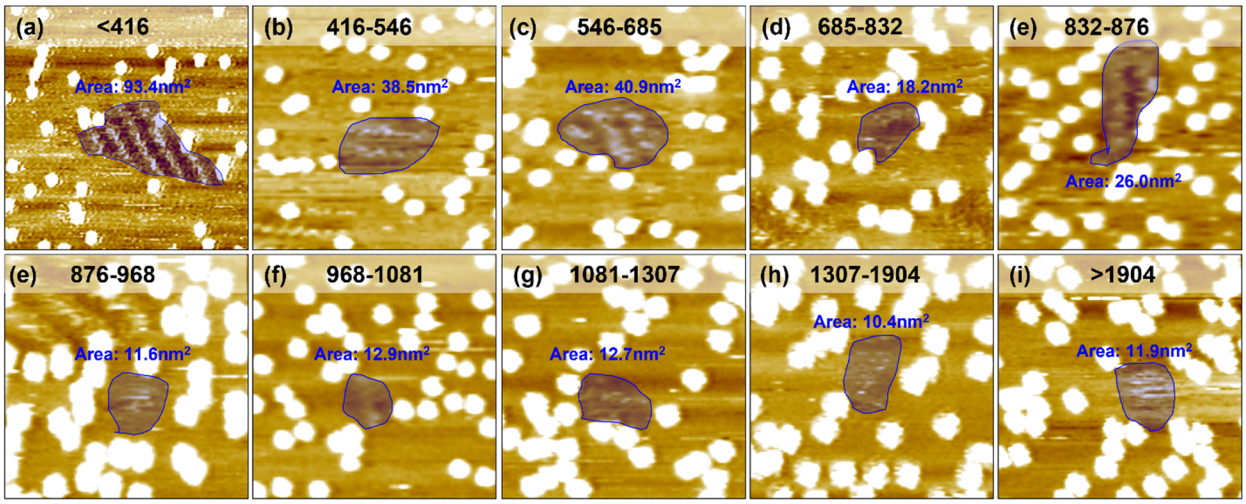

Figure S6. STM images of the smallest domains of QZ-C16 assembly (at concentration 10^{-6} M) on the CM-HOPG surface at 10 groups of grafting densities.

Table S5. Minimum domain size obtained at 10 groups of grafting densities. The number of surrounding grafts and the size of domains in the previous image or later image are provided.

Row #	Grafting density (pins/per 0.01 μm²)	Minimum domain size (nm²)	Number of surrounding grafts	Domain size of previous image (nm²)	Domain size of later image (nm²)
1	<416	93.4	7	-	281.0
2	416-546	38.5	4	-	unclear
3	546-685	40.9	7	104	0
4	685-832	18.2	7	unclear	17.3
5	832-876	26.0	10	-	31.3
6	876-968	11.6	7	0	0
7	968-1081	12.9	4	-	-
8	1081-1307	12.7	7	-	0
9	1307-1904	10.4	8	unclear	0
10	>1904	11.9	6		0

To narrow down the experimentally estimated range of critical nuclei, the following argumentation rational can be used:

1) Let us assume that grafts do provide significant, non-negligible favorable interactions to QZ-C16 assembly (actually, assuming that this is not the case immediately suggests that 10.40 nm² is the upper experimental estimate of a QZ-C16 critical nuclei);

2) Let us also assume that every graft provides equally large stabilizing interactions to QZ-C16 assemblies;

3) Under assumptions (1) and (2), the comparison of data in rows #1, #3, #4, #6 and #8 will not involve the influence of grafts since each of the smallest domains in those selections had exactly 7 grafts in contact with QZ-C16 domains;

4) To decrease the upper experimental estimate of the critical nucleus size we should choose between 93.4 nm^2, 40.9 nm^2, 18.2 nm^2, 11.6 nm^2 and 12.7 nm^2. We propose 18.2 nm^2 (row #4) only because it is the smallest domain in this selection that has been observed for at least 90 seconds (in consecutive images we still observed self-assembly here). There is no practical benefit for this work to identify the critical nucleus size of QZ-C16 assembly more precisely. For our discussions, it is sufficient to estimate the critical nucleus size in the range of 10-18 nm^2 and state that all domains larger than this had also undergone a "growth" stage.

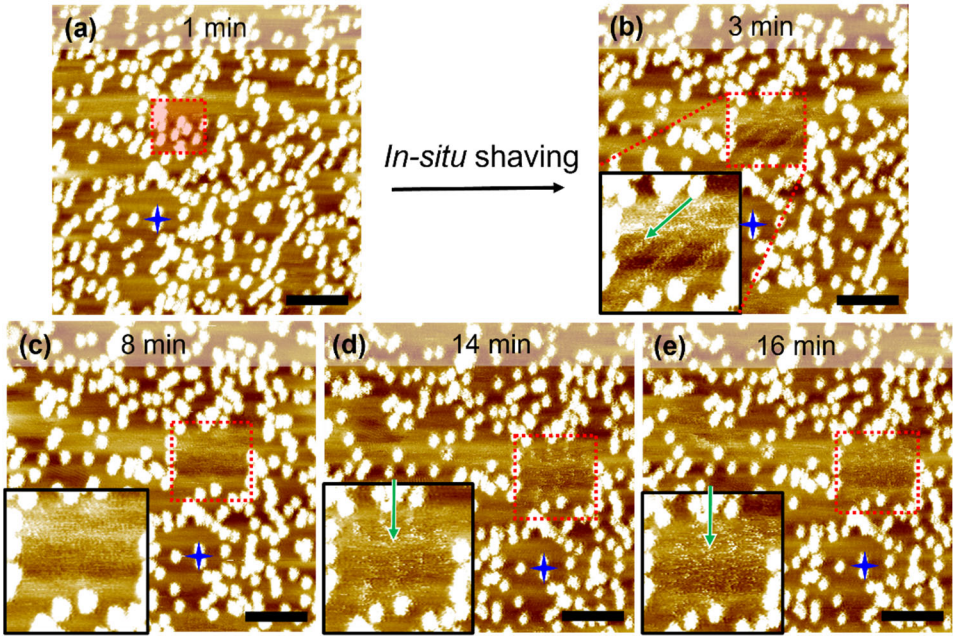

Figure S7. (a) No QZ-C16 assemblies were observed on the CM-HOPG surface (at concentration 10^{-6} M). Then STM was operated at a high current (0.2 nA) and low sample bias (–0.001 V) to bring the tip very close to the substrate surface, the *in-situ* shaving procedure was subsequently conducted in the red square area, around 13 pins were removed from the surface and a corral with a size of 9 ×11 nm was created. Nanoshaving was performed using the PicoLITH v.2.1 software. (b) The QZ-C16 molecules could immediately assemble inside the manipulatively formed corral. (c-e) The structure and orientation of assemblies inside the corral changed over a 16-minute period because of the continuous adsorption/desorption dynamic process. The green arrow indicates the orientation of assemblies. The blue stars provide reference points in sequential images. Scale bars: 10 nm.

S3. Dynamic processes of QZ-C16 assembly under confinement space.

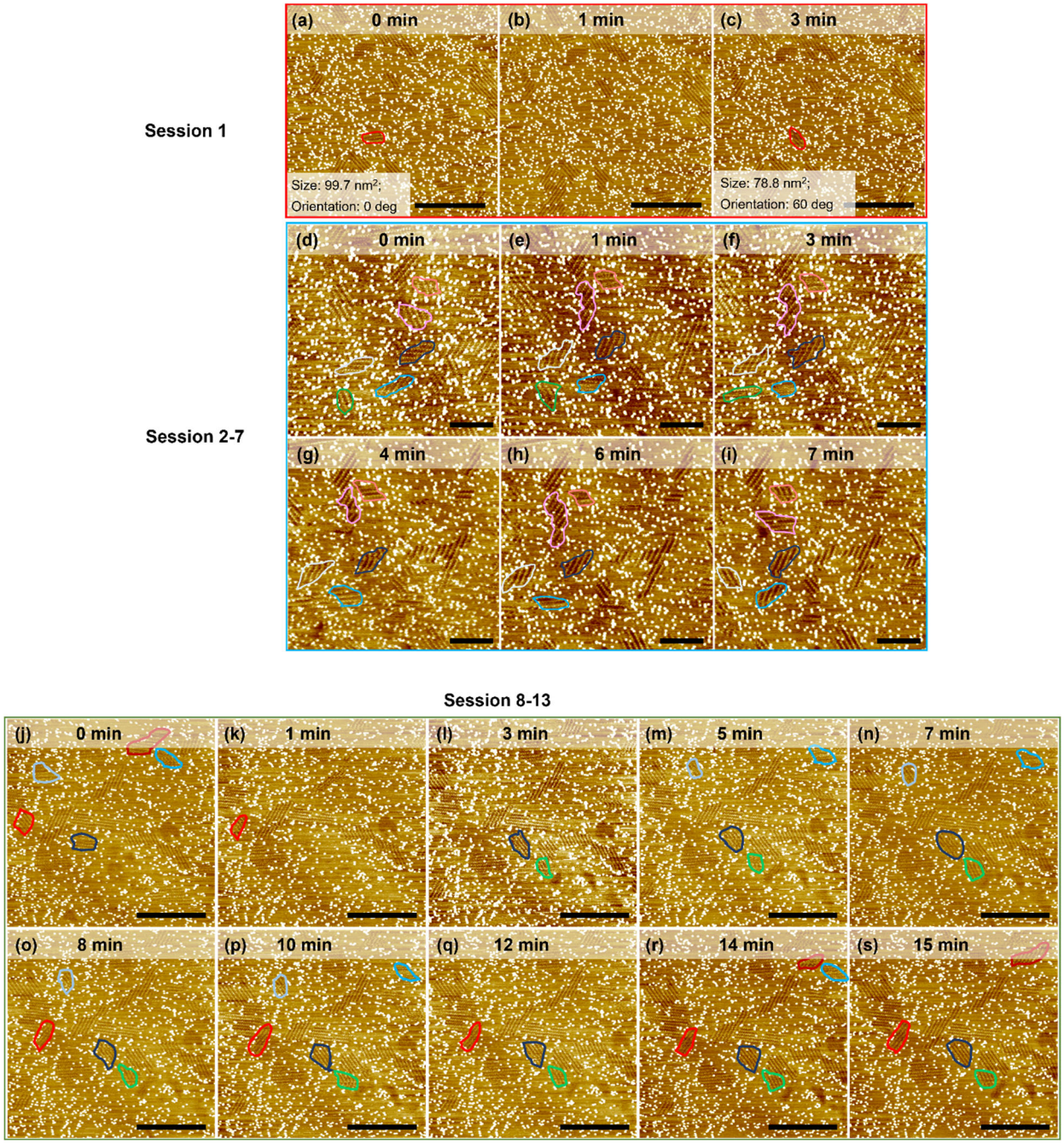

Figure S8. Three groups (a-c, d-i and j-s) of sequential images show in total 13 sessions of dynamic processes during short instant scanning. Different sessions are highlighted in different colors. Scale bars: 20 nm. Imaging parameters: $V_s = -0.8$ V, $I_t = 0.08$ nA.

Table S6. Statistics of the size and orientation changes of QZ-C16 (10^{-6} M) domains on the CM-HOPG for a total of 12 sessions of dynamic processes shown in Figure S7 d-s.

Time (min)	Session 2 (Rose)		Session 3 (Lavender)		Session 4 (Dark blue)		Session 5 (Blue)		Session 6 (White)		Session 7 (Green)	
	Size (nm^2)	Orientation (Deg)	Size (nm^2)	Orientation (Deg)	Size (nm^2)	Orientation (Deg)	Size (nm^2)	Orientation (Deg)	Size (nm^2)	Orientation (Deg)	Size (nm^2)	Orientation (Deg)
0	81.2	60	125	70	96.7	0	92.2	-60	68.8	0	66.8	60
1	64.1	0	272	-60	105.0	-60	81.1	0	98.2	-60	82.8	60
3	61.6	0	323	-60	114.0	-60	64.8	0	92.1	-60	70.7	0
4	66.4	0	191	-60	93.6	-60	73.6	0	71.4	-60		
6	65.0	0	260	-60	86.7	-60	74.7	0	74.1	-60		
7	75.5	60	120	0	90.3	-60	73.6	-60	65.7	60		

Time (min)	Session 8 (Dark red)		Session 9 (Blue)		Session 10 (Light blue)		Session 11 (Red)		Session 12 (Dark blue)		Session 13 (Green)	
	Size (nm^2)	Orientation (Deg)	Size (nm^2)	Orientation (Deg)	Size (nm^2)	Orientation (Deg)	Size (nm^2)	Orientation (Deg)	Size (nm^2)	Orientation (Deg)	Size (nm^2)	Orientation (Deg)
0	229.0	0	122.0	un	123.0	0	143.0	55	156.0	0	-	-
1	0	-	0	-	0	-	91.1	55	0	-	-	-
3	0	-	0	-	0	-	0	-	177.0	60	95.5	70

5	0	-	129.0	0	95.9	50	0	-	156.0	60	81.8	un
7	0	-	118.0	0	131.0	50	0	-	196.0	60	144.0	70
8	0	-	154.0	0	84.7	50	186.0	-50	194.0	60	148.0	70
10	0	-	144.0	0	85.7	50	144.0	-50	164.0	60	137.0	70
12	0	-	162.0	0			167.0	-50	175.0	60	134.0	70
14	112.0	90	124.0	un			150.0	-50	185.0	60	128.0	70
15	257.0	-65					172.0	-50	175.0	60	222.0	70